eJSSNT Regular Paper

e-Journal of Surface Science and Nanotechnology **23**, 306–313 (2025)

Atomic Scale Insights into Si Transport Pathway in Si-oxide Film Based on Theoretical Investigation of Medium Density Effects

Hiroyuki Kageshima,[a, †] Toru Akiyama,[b] Kenji Shiraishi [c, d]

[a] *Graduate School of Natural Science and Technology, Shimane University, 1060 Nishi-Kawatsucho, Matsue, Shimane 690-8504, Japan*
[b] *Graduate School of Engineering, Mie University, 1577 Kuriya-Machiya, Tsu, Mie 514-8507, Japan*
[c] *Institute of Materials and Systems for Sustainability, Nagoya University, Furo-cho, Chikusa-ku, Nagoya, Aichi 464-8603, Japan*
[d] *Graduate School of Engineering, Nagoya University, Furo-cho, Chikusa-ku, Nagoya, Aichi 464-8603, Japan*
[†] *Corresponding author: kageshima@riko.shimane-u.ac.jp*

Received: 5 February, 2025; Accepted: 11 June, 2025; J-STAGE Advance Publication: 17 July, 2025; Published: 17 July, 2025

To elucidate the effect of medium strain on silicon (Si) transport in Si oxides, first-principles calculations were employed to evaluate the variation in the diffusion barrier of excess Si in isotropically strained quartz. Our results reveal that the barrier height exhibits significant dependence on density. The optimal barrier height, determined from the most stable metastable structure and the lowest transition state structure, was found to be 5.06 eV, in excellent agreement with the experimental value of 5.13 eV. Furthermore, a detailed analysis of experimental Si diffusion coefficients suggests that oxide films used in experiments can be categorized into at least two distinct types. This finding underscores the necessity of classifying oxide films based on structural characteristics rather than treating them as a single amorphous phase, ensuring a more precise understanding of their quality.

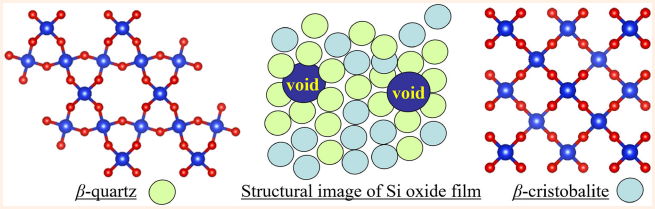

Keywords *MOS interface; Silicon oxidation; First-principles calculation*

I. INTRODUCTION

The silicon (Si) metal-oxide-semiconductor (MOS) interface is a fundamental and critical component in both conventional and emerging electronic devices. MOS field effect transistors (MOSFETs), widely used in logic circuits, memory, analog devices, and imaging sensors, rely on the integrity of this interface. Moreover, next-generation technologies, including electron fluid effect devices [1] and Si MOS-based qubits for quantum computing, also depend on its performance [2]. However, surface roughness [3] and charge trapping sites at the MOS interface are primary sources of device degradation [4–6]. Charge trapping sites, often referred to as floating or fixed charges, originate from defects such as E_1' centers in the oxide layer, hot-carrier-induced defects, and P_b centers at the interface. Additionally, oxygen (O) vacancies (V_O) in the oxide layer present significant reliability challenges, contributing to gate leakage currents and potentially leading to dielectric breakdown [7, 8].

Most of these defects originate during the formation of the MOS interface in the oxidation process. Since the interface is created through the thermal oxidation of Si, achieving an atomic-scale understanding of this process is essential for precise control over interface properties. Given its critical role in MOSFETs, the Si MOS interface must exhibit high electrical inertness. However, phenomena such as oxidation-induced stacking faults (OSF) [9] and oxidation-enhanced/reduced diffusion (OED/ORD) [10] indicate that excess Si can be generated at the interface during oxidation, potentially incorporating into the Si oxide film [11, 12].

Therefore, we theoretically investigated the transport process of Si from the MOS interface into the Si oxide film [13, 14]. Using a quartz interface model, where the quartz oxide film is structurally deformed to match the Si(001) substrate surface, we identified the transport pathway of excess Si into the oxide film. First-principles calculations determined the energy barrier for this transport to be 4.55 eV, which is rather in good agreement with the experimental value of 5.13 eV.

Furthermore, by applying the 4.55 eV barrier height and evaluating the diffusion coefficient using a simple transition state theory, we found that assuming a hopping length of approximately 100 Å successfully reproduces the experimental results.

The successful reproduction of experimental results using quartz as a model for the oxide film suggests that quartz-like regions exist within actual Si oxide films and likely govern the rate-limiting process of Si transport. However, while the density of Si oxide films is 2.2 g cm^{-3}, our interface model's oxide film has a density of 2.27 g cm^{-3}, compared to 2.54 g cm^{-3} for unstrained β-quartz. Moreover, since actual Si oxide films are amorphous, significant local density fluctuations are expected. This suggests that quartz-like regions with varying densities exist within Si oxide films, serving as pathways for excess Si transport. Given this, an important question arises: how does the density of the quartz medium influence the energy barrier for excess Si transport?

In this study, we systematically investigated this problem. Our previous work showed that the energy barrier for excess Si diffusion in unstrained β-quartz (density: 2.54 g cm^{-3}) was 4.65 eV, closely matching the result from our interface model with an oxide film density of 2.27 g cm^{-3} [13, 14]. To further explore this dependence, we generated quartz structures with varying densities by isotropically expanding and compressing quartz and evaluated the energy barrier for excess Si diffusion in each case. Our results reveal a strong correlation between barrier height and density. The optimal barrier height, determined from the most stable metastable structure and the lowest transition state structure, was 5.06 eV, remarkably close to the experimental value of 5.13 eV [15]. Furthermore, a detailed analysis of Si-related diffusion coefficients in experimental oxide films suggests that these films can be classified into at least two distinct types. This finding underscores the need to treat oxide films not as a uniform amorphous phase but rather as a collection of structurally distinct regions, necessitating a more refined classification for quality control.

II. METHODS

We investigated the transport process of excess Si in SiO_2 with various densities using first-principles calculations. These calculations were performed based on density functional theory (DFT) using the PHASE/0 code [16, 17]. A plane-wave basis set with a cutoff energy of 30 Ry was employed. For pseudopotentials, an ultrasoft pseudopotential was used for O [18], while a norm-conserving pseudopotential was used for Si. The exchange-correlation functional was treated using the generalized gradient approximation (GGAPBE) [19].

The computational model was based on the $2 \times \sqrt{3} \times 2$ supercell of β-quartz, which was also used in our previous study [13, 14]. The relaxed unit cell of β-quartz reported previously was directly adopted, corresponding to a density of 2.54 g cm^{-3}. In this case, the lattice constants of the *a*-, *b*-, and *c*-vectors were 9.99, 10.91, and 8.65 Å, respectively [Figure 1(a)]. In the present study, considering that the typical density of Si oxide films is 2.22 g cm^{-3}, we examined six different densities ranging from 2.96 to 2.04 g cm^{-3}. The relaxed unit cell of α-quartz corresponded to a density of 2.65 g cm^{-3}. Next, the β-quartz unit cell was isotropically scaled by factors of 0.95, 1.02, 1.035, 1.05, and 1.075, corresponding to densities of 2.96, 2.39, 2.29, 2.19, and 2.04 g cm^{-3}, respectively. In the interface model, which we employed in the previous study [13], the lattice constants of the oxide film region were strained by +8.7%, −0.5%, and +3.3% in comparison to relaxed β-quartz, resulting in a density of 2.21 g cm^{-3}. A Monkhorst-Pack 4 × 4 × 4 *k*-point sampling was applied [20].

In this study, we assume, as in our previous work, that excess Si is transported in the form of SiO interstitial (I_{SiO}), where Si is accompanied by an O atom [13, 14]. The transport pathway considered here follows the same mechanism reported in our previous research, constructed based on three fundamental processes: (1) V_O transfer (VOT), (2) Si coordination number conversion (CNC), and (3) ACBD bond-order conversion (BOC).

The details of VOT, CNC, and BOC processes are presented in Figure 4 of Ref. 13. The VOT corresponds to the migration of a V_O to a neighboring site. Since a V_O site effectively represents a Si–Si bond within the Si–O–Si network, the VOT process can be regarded as the reverse transition process of an O atom moving from a neighboring site into the vacancy. During VOT, only an O atom is displaced, while the positions of Si atoms remain nearly unchanged. The CNC process involves the interconversion between the 2- and 4-coordinated SiO structures, accompanied by significant displacement of Si atoms. In contrast, the BOC process entails a reconfiguration of bonding involving two O and two Si atoms, resulting in positional change of both species. Notably, Si atoms are displaced only during CNC and BOC events. However, VOT plays a critical role in facilitating these transitions by repositioning the V_O to favorable locations. Consequently, although Si transport occurs through sequence of CNC and BOC processes, there are interconnected by a series of VOT events. Therefore, the overall Si transport mechanism is effectively constructed from a network of CNC and BOC transitions mediated by frequent VOT events.

As in our previous study, we constructed a full pathway for excess Si transport to a neighboring equivalent site that is related to the start site by a translation of one lattice vector. The atomic structures corresponding to the start and the goal configurations are shown in Figure 1(b, c). The full pathway consists of 8 VOT processes, 11 CNC processes, and 1 BOC process. The current pathway exhibits slight modification compared to those reported previously. Following the publication of Ref. 13, which describes only the metastable structures along the pathway, we conducted further analysis of associated transition state structures. This revealed that some metastable structures previously identified in Ref. 13 were not entirely appropriate for the pathway. Specifically, the original metastable structure shown in Image 5 must be

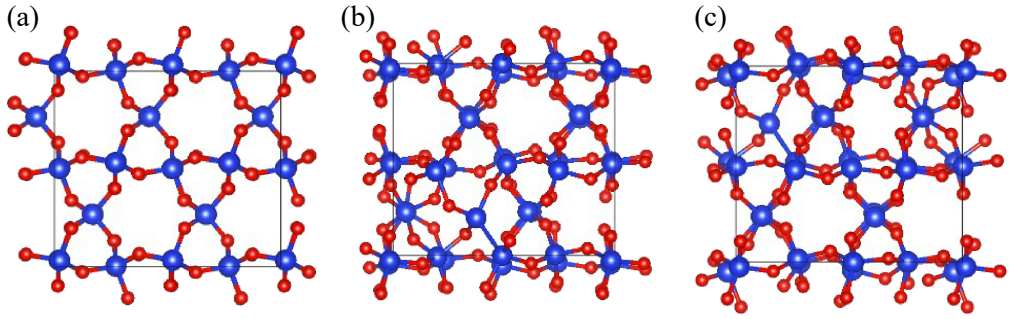

Figure 1: (a) Atomic structure on the unit cell of $2 \times \sqrt{3} \times 2$ supercell model based on relaxed β-quartz. Atomic structures of (b) the start (Image 0) and (c) the goal (Image 120) of the Si transport path we considered. An I_{SiO} is transported in this path. Blue and red spheres represent Si and O atoms, respectively.

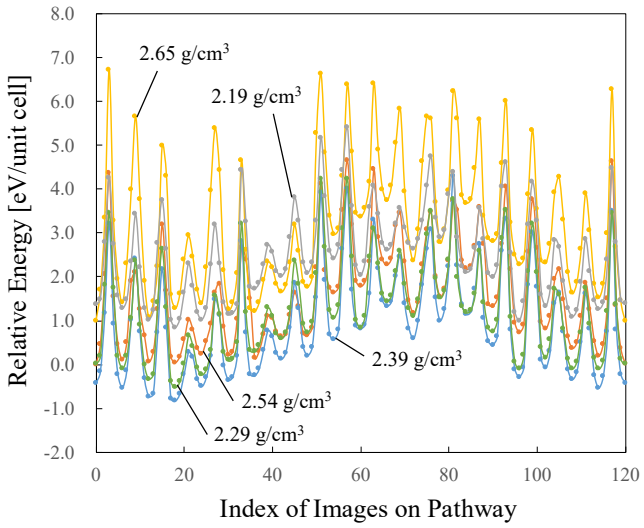

Figure 2: Medium-density dependence of energy profile on the pathway of I_{SiO} transport. The energy origin is chosen as the energy of Image 0 at a density of 2.54 g cm^{-3}.

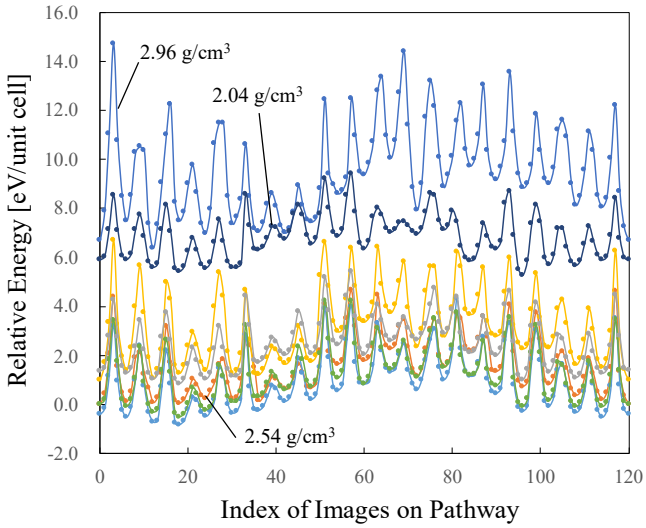

Figure 3: Wider medium-density dependence of energy profile on the pathway of I_{SiO} transport. The energy origin is chosen as the energy of Image 0 at a density of 2.54 g cm^{-3}.

revised, the original metastable structure in Image 8 must be removed, and a metastable structure from Image 9 must also be modified and reassigned as the new metastable structure corresponding to Image 8. Consequently, the number of metastable structures is reduced from 20 as shown in Figure 8 of Ref. 13 to 19 in Figure 5 of Ref. 14. However, subsequent investigation revealed that the metastable structure of the goal presented in Ref. 14 does not possess the necessary translational equivalence to the start site, although it is surely stable as the exact goal. An additional VOT step is therefore required to complete the pathway. As a result, the total number of metastable structures in the present study returns to 20. As in our prior study, we evaluated the energy barriers between successive metastable structures along this pathway using the climbing image nudged elastic band (CI-NEB) method.

III. RESULTS AND DISCUSSIONS

The calculated energy variations associated with Si transport in strained quartz are presented in Figure 2. The energy origin is chosen as the energy of Image 0 at a density of 2.54 g cm^{-3}. Image 0, shown in Figure 1(b), corresponds to the start metastable structure in the path of I_{SiO} transport. The results confirm that density fluctuations significantly influence variations in energy. Furthermore, the calculation results over a wider range of densities are presented in Figure 3. The results as a function of density are summarized in Figure 4, including individual images, the highest energy along the entire pathway, the lowest energy along the entire pathway, and the maximum energy barrier. The details of atomic structures of individual images are shown in Figure 5.

Among these, Image 0 and Image 18 correspond to metastable structures, while Images 3, 57, and 81 represent transition state structures. Most energy profiles exhibit a convex downward shape with a minimum at 2.39 g cm^{-3}. However, Image 81 deviates from this trend, displaying a W-shaped profile with local minima at 2.29 and 2.54 g cm^{-3}. The images corresponding to the highest energy along the entire pathway are as follows: Image 3 (VOT) at 2.96 and 2.65 g cm^{-3}, Image 57 (VOT) at 2.54 g cm^{-3}, Image 81 (CNC 2-coordination formation) at 2.39 g cm^{-3}, Image 51 (VOT) at

2.29 g cm^{-3}, and Image 57 (VOT) at 2.19 and 2.04 g cm^{-3}. Conversely, the images corresponding to the lowest energy along the entire pathway are: Image 12 at 2.96 g cm^{-3}, Image 0 at 2.65 and 2.54 g cm^{-3}, Image 18 at 2.39, 2.29, and 2.19 g cm^{-3}, and Image 96 at 2.04 g cm^{-3}. The maximum energy barrier along the entire pathway varies with density, reaching 8.34 eV at 2.96 g cm^{-3}, 5.70 eV at 2.65 g cm^{-3}, 4.65 eV at 2.54 g cm^{-3} (corresponding to unstrained β-quartz), 5.25 eV at 2.39 g cm^{-3}, 4.75 eV at 2.29 g cm^{-3}, 4.56 eV at 2.19 g cm^{-3}, and 4.16 eV at 2.04 g cm^{-3}.

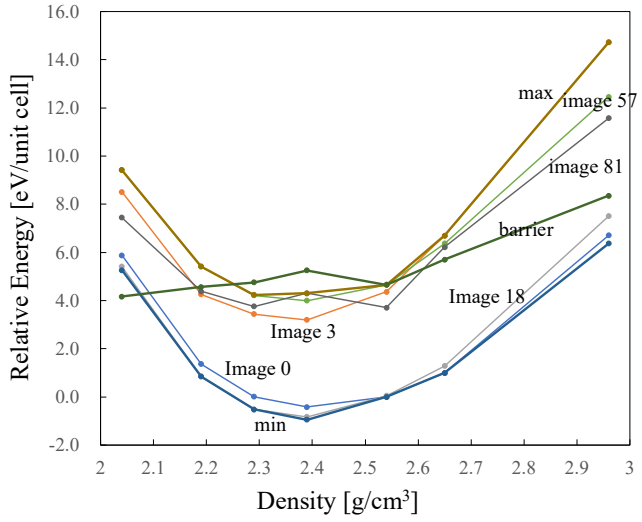

Figure 4: Medium-density dependence of energies for some images on the Si transport path (Image 0, Image 3, Image 18, Image 57, Image 81), the minimum energy on the path (min), the maximum energy on the path (max), and the barrier height calculated from the difference between min and max (barrier).

Notably, the maximum energy barrier generally increases with density, reaching a local maximum at 2.39 g cm^{-3}, decreasing to a local minimum at 2.54 g cm^{-3}, and subsequently increasing again. Furthermore, within the calculated density range, the lowest maximum energy along the entire pathway is 4.23 eV at 2.29 g cm^{-3}, while the lowest minimum energy along the pathway is −0.83 eV at 2.39 g cm^{-3}. In addition, we just considered a scenario in which the Si oxide film is composed of quartz-like regions with varying densities. In this context, we assumed that excess Si transport is rate-limiting by the transport path beginning from the region with the most stable metastable state and proceeding through the region characterized by the lowest maximum energy barrier. We refer to the barrier of this path as the optimal estimated barrier height. Assuming a mixture of densities within this range, the optimal estimated barrier height is 5.06 eV, which closely matches the experimental value of 5.13 eV [15].

Using these calculated barrier heights, we evaluated the diffusion coefficient based on a simple transition state theory [14]. The diffusion coefficient is calculated as

$$D = \frac{a^2}{n}\frac{k_B T}{h}\exp\left(-\frac{E_B}{k_B T}\right), \quad (1)$$

where E_B is the barrier height, T the temperature, k_B the Boltzmann constant, h the Planck constant, $n = 6$ the number of diffusion direction, and a the hopping distance. The results obtained with the optimal barrier height of 5.06 eV and the barrier height of 4.65 eV at 2.54 g cm^{-3} (unstrained β-quartz) are presented in Figure 6, along with previous results for reference. Although experimental values exhibit significant

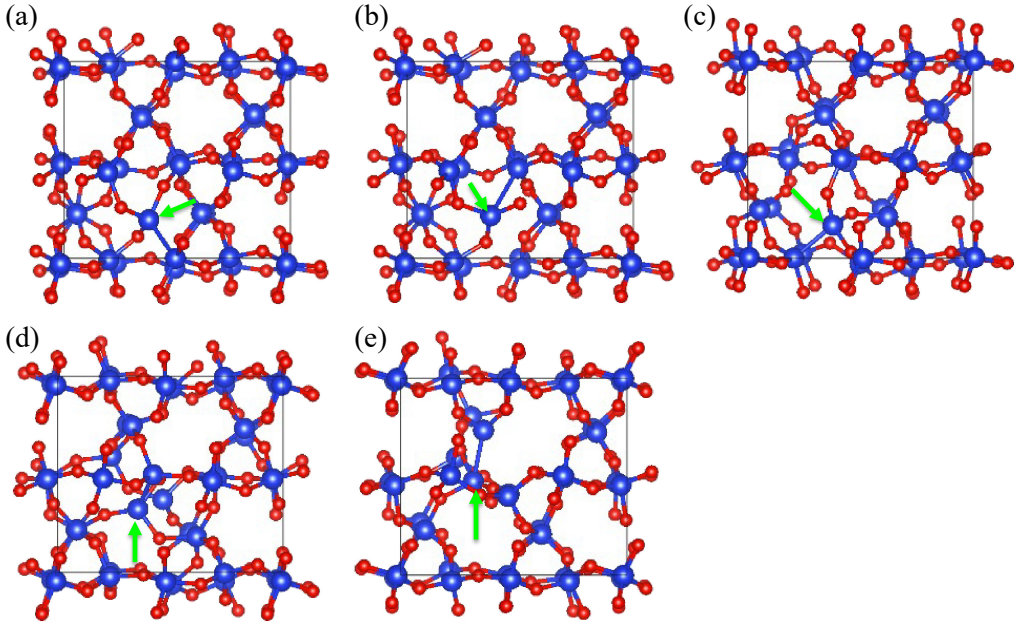

Figure 5: Atomic structures for the images described in Figure 4. (a) Image 0, (b) Image 3, (c) Image 18, (d) Image 57, and (e) Image 81. Images 0 and 18 are metastable structures, while Images 3, 57, and 81 are transition state structures. Excess Si atoms are indicated by green arrows.

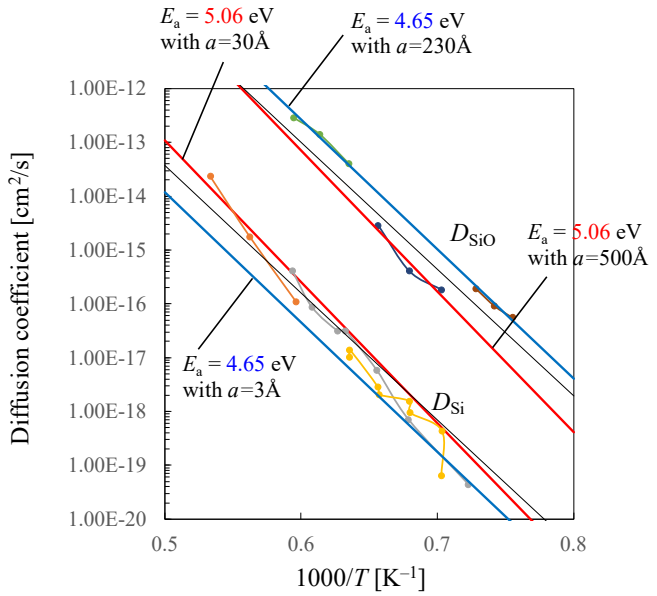

Figure 6: Comparison of diffusion coefficients evaluated from our theoretical results with experiments. Blue and red solid straight lines are coefficients evaluated from activation energy of 4.65 and 5.06 eV, respectively. Solid lines with dots are coefficients reported by experiments [15]. Black solid straight lines are theoretical coefficients we previously reported [14]. D_{SiO} and D_{Si} represent the diffusion coefficients of SiO and Si, respectively.

variation, this variability likely arises from differences in Si oxide quality, which influence the activation energy. For instance, the diffusion coefficient of SiO (D_{SiO}) can be categorized into two groups: one with an activation energy of E_a = 4.65 eV and a hopping length of a = 230 Å, and another with E_a = 5.06 eV and a = 500 Å. Similarly, for the diffusion coefficient of Si, two distinct groups emerge: one with E_a = 5.06 eV and a = 30 Å, and another with E_a = 4.65 eV and a = 3 Å, although the underlying reasons remain unclear. These findings suggest that amorphous Si oxides can be classified into at least two distinct types: one where Si transport is rate-limited by unstrained β-quartz-like regions, and another where transport is governed by two different types of tensile-strained quartz-like regions.

The successful reproduction of experimental results on excess Si transport using quartz as a model for the oxide film suggests that quartz-like regions are indeed present within actual Si oxide films and play a key role in governing Si transport. However, while real Si oxide films are amorphous, they are known to exhibit, on average, a cristobalite-like structural character [21]. Additionally, amorphous Si oxides contain voids of varying sizes, with larger voids being less common yet still present [22–28]. One possible explanation for the variation in hopping lengths is the variation of size and density of voids in the oxide, because we can imagine that the excess Si is stable at these voids and hops between them when it transports through the oxide. These considerations indicate that Si oxide films are not purely amorphous but rather complex composites—predominantly cristobalite-like on average, interspersed with quartz-like regions and voids, thus exhibiting a degree of structural order (Figure 7). Therefore, while we have not yet studied the Si transport in cristobalite or around voids, we need to consider deeply about the composition or quality of Si oxide.

Cristobalite and quartz are distinct structural phases of SiO_2. The density of Si oxide films is 2.2 g cm^{-3}, compared to 2.21 g cm^{-3} for cristobalite and 2.54 g cm^{-3} for quartz. While quartz is the most stable phase at room temperature and pressure, cristobalite can form simply just only by inserting O atoms between Si–Si bonds in a Si crystal. Based on density considerations, if the oxide film is a composite of three phases, high-density quartz-like regions and low-density void regions are considered to exist to the same extent.

However, when Si is converted into cristobalite at the interface just only by the O insertion between Si–Si bonds of the Si substrate, the density of formed cristobalite is 2.64 to 2.86 g cm^{-3} [26], which is quite larger than the density of relaxed Si oxide films of 2.2 g cm^{-3}. Therefore, during the Si oxidation process, the formed Si oxide at the interface should be relaxed by some mechanisms. In this context, it is noteworthy that a highly compressed cristobalite can be converted into a relaxed cristobalite via quartz by emitting excess Si repeatedly. Certainly, cristobalite can transform into quartz by periodically removing SiO_4 units, shrinking the structure by a factor of 0.65, and inserting O atoms (Figure 8) [11, 29]. Conversely, quartz can convert into cristobalite by periodically removing O atoms, expanding the structure by a factor of 1.53, and inserting SiO_4 units. Additionally, cristobalite can transition to quartz by periodically removing SiO_4 units, shrinking by a factor of 0.77, and inserting O atoms (Figure 9), whereas quartz can be converted to cristobalite by periodically removing O atoms, expanding by a factor of 1.30, and inserting SiO_4 units. Such

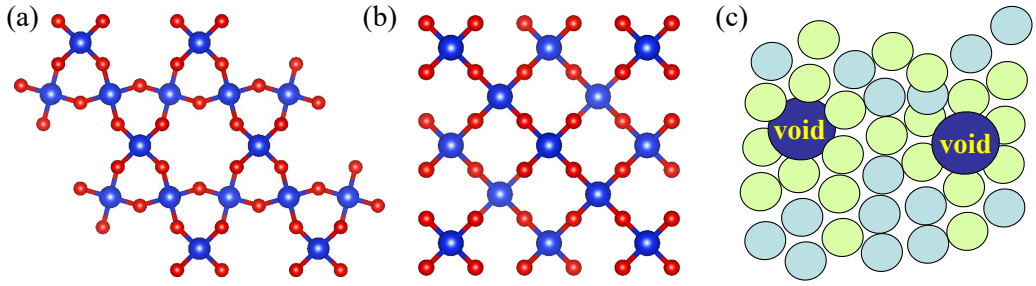

Figure 7: Atomic models related to the Si oxide. (a) β-quartz, (b) β-cristobalite, and (c) schematic image for the Si oxide layer we propose.

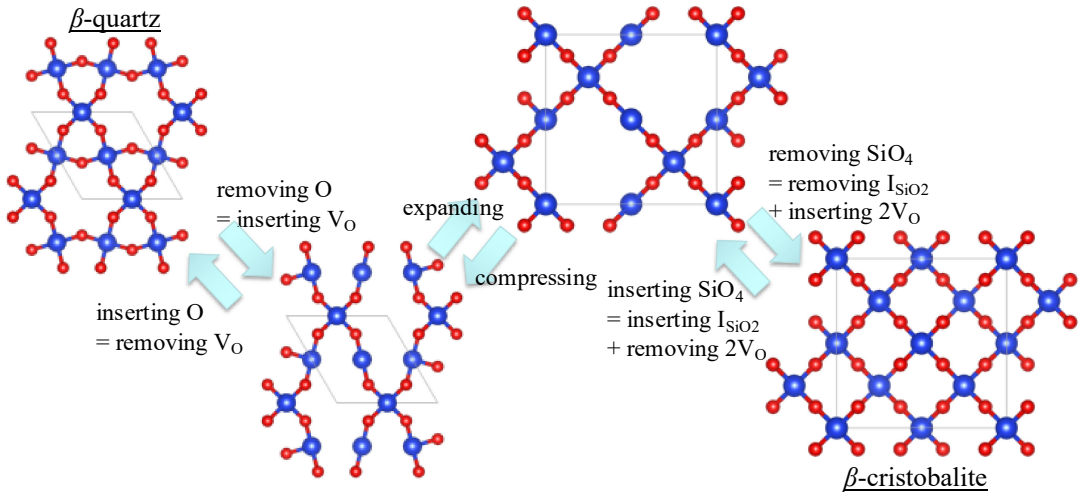

Figure 8: One path for converting β-quartz into β-cristobalite just only by inserting or removing excess Si and O.

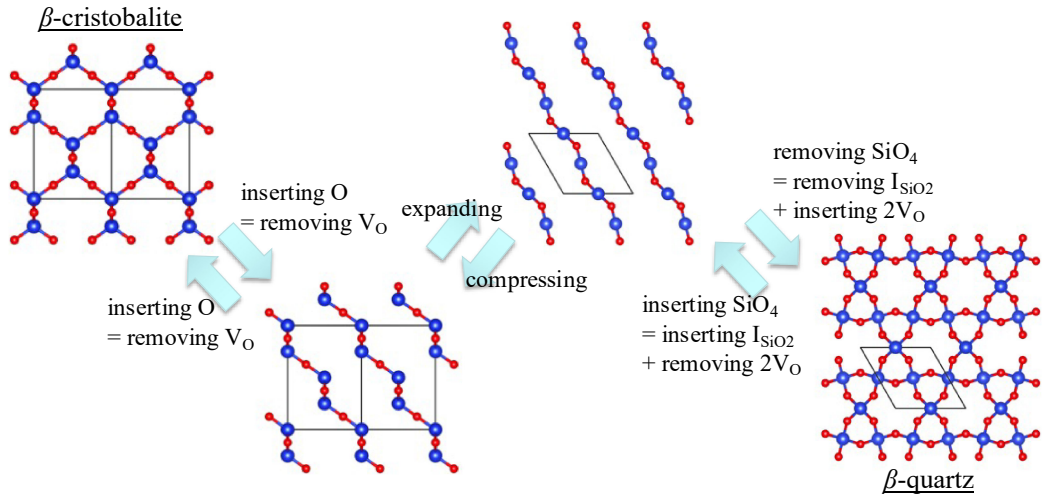

Figure 9: Another path for converting β-cristobalite into β-quartz just only by inserting or removing excess Si and O.

structural conversion would happen not only in Si oxide formed by the oxidation, but also even in mere amorphous Si oxide due to the thermal fluctuation in some extent.

These structural transformations are governed by the insertion and removal of SiO_2 interstitials (I_{SiO2}) and V_O. Removing SiO_4 units corresponds to the removal of I_{SiO2} and the simultaneous insertion of two V_O, while inserting SiO_4 units requires inserting I_{SiO2} and removing two V_O. The insertion of V_O corresponds to O removal, whereas V_O removal corresponds to O insertion. Similarly, I_{SiO2} insertion corresponds to SiO_2 vacancy (V_{SiO2}) removal, and I_{SiO2} removal corresponds to V_{SiO2} insertion. By periodically inserting I_{SiO2} into quartz, the density increases to 3.39 g cm^{-3}, whereas removing I_{SiO2} from cristobalite reduces the density to 1.66 g cm^{-3}. Inserting I_{SiO2} into cristobalite results in a density of 2.87 g cm^{-3}, while removing I_{SiO2} from quartz decreases the density to 1.95 g cm^{-3}.

I_{SiO2} represents excess Si, while aggregates of V_{SiO2} correspond to voids. Given that Si undergoes a volumetric expansion by a factor of 2.25 during oxidation, it follows that the transport of excess Si, along with the aggregation and dispersion of V_{SiO2}, plays a crucial role in determining the structure and quality of Si oxide films formed via thermal oxidation. For both D_{SiO} and D_{Si}, there is a clear trend where a larger activation energy E_a corresponds to an increased hopping length a. This correlation can be attributed to excess Si hopping between voids. Specifically, when excess Si migrates through larger voids, it attains greater stability within these voids, leading to a higher E_a. Furthermore, since larger voids are less common, the hopping length naturally increases in such cases.

Moreover, not only D_{SiO}, which is expected to be determined by the transport of excess Si, but also D_{Si}, which corresponds to Si self-diffusion where excess Si is not necessarily assumed to be present, can be explained using the energy barriers for excess Si transport in quartz. This suggests that Si self-diffusion is also governed by excess Si transport as the rate-limiting process. To generate excess Si

within a homogeneous Si oxide, temporary formation of vacancies such as V_{SiO2} is required. However, amorphous Si oxide films likely contain pre-aggregated regions of excess Si, such as high-density cristobalite or high-density quartz. In this case, the dispersion of excess Si from these regions could serve as the rate-limiting process for D_{Si}, which aligns well with our findings. Furthermore, the hopping length required to reproduce D_{Si} ranges from 3 to 40 Å, approximately 1/20 to 1/80 of that for D_{SiO}. This observation is consistent with the idea that amorphous Si oxide films contain pre-existing regions of aggregated voids, such as low-density cristobalite or low-density quartz. In contrast, since D_{SiO} involves the transport of externally introduced excess Si, it is reasonable to assume that it is associated with extremely rare, large voids. These considerations support our hypothesis that the Si oxide films are not uniformly amorphous but can instead be regarded as complex, nonuniform composites.

In this context, the decrease in the maximum energy barrier as the density increases from 2.39 to 2.54 g cm^{-3} is qualitatively consistent with previous theoretical calculations on liquid or amorphous, which suggest that the viscosity of Si oxides decreases under compression [30, 31]. This reduction in viscosity is likely driven by an increase in the D_{Si} rate. However, estimating the stress variation based on the total energy change during this process yields an approximate change of 9 GPa. From this, the activation volume for the diffusion barrier height is estimated to be around 9×10^3 Å^3, which is significantly larger than the experimental value of approximately 200 Å^3 [32].

It is important to note that since experimental Si oxide films are amorphous, estimating the activation volume under the assumption of a crystalline structure introduces inherent uncertainties, likely contributing to the observed discrepancy with experimental values. Additionally, comparing the calculated diffusion barrier height of I_{SiO} with the activation energy of the actual Si self-diffusion coefficient may not be entirely appropriate. Conversely, in other density regimes of our calculated results, D_{Si} slows under compression, which qualitatively contradicts previous theoretical predictions. Nevertheless, at the very least, these findings provide some insights into the structural and transport properties of Si oxide films, warranting further detailed investigation, as discussed above. The similarity in which transport is enhanced by compression may be coincidental, but we think it is noteworthy and point it out here. We believe that the large difference in activation volume is due to the comparison of liquid and amorphous phenomena with crystalline structures.

In this study, we assumed, consistent with our previous analyses, that excess Si is transported in the form of I_{SiO} with accompanying O [13, 14]. Based on this assumption, we calculated the energy barriers for Si transport. This assumption was necessary because, without considering I_{SiO}, the three elementary processes, VOT, CNC, and BOC, would not be valid, leading to significantly higher energy barriers for excess Si transport. However, the successful reproduction of experimental results for both D_{SiO} and D_{Si} suggests that this assumption might be reasonable.

This finding implies that neither the formation nor the transport of V_O serves as a rate-limiting step. It is likely that pre-existing voids in amorphous Si oxide films facilitate V_O formation. Furthermore, our previous theoretical study showed that the energy barrier for V_O transport in strain-free β-quartz at a density of 2.54 g cm^{-3} is 4.56 eV, whereas in 10% tensile-strained quartz with a density of 1.91 g cm^{-3}, the barrier is significantly lower at 2.86 eV [33]. Since these values are much lower than the energy barrier for I_{SiO} transport, V_O transport is unlikely to be the rate-limiting step.

Based on these considerations, amorphous Si oxide films can be consistently understood as heterogeneous mixtures of regions with aggregated excess Si and regions with clustered voids, each exhibiting distinct densities. Therefore, rather than treating Si oxide films as uniformly amorphous, it is essential to classify their quality based on the density distributions of excess Si-rich and void-rich regions. Such a classification would enable a more systematic interpretation of experimental results. Additionally, previous reports indicate that the density, structure, and quality of Si oxide films vary between the interface region and more distant regions [34, 35]. This underscores the need for further in-depth investigations from both experimental and theoretical perspectives.

In this study, we have just only studied the excess Si transport in different density quartz. If the Si oxide can surely be regarded as the composite of quartz, cristobalite, and voids as discussed above, it is highly required to study the excess Si transport in various density cristobalite and around various size voids. These are left for the future work.

IV. CONCLUSIONS

To investigate the effect of strain in the medium on Si transport in Si oxides, we performed first-principles calculations to evaluate the changes in the diffusion barrier of I_{SiO} in isotropically strained quartz. The results revealed that the diffusion barrier height exhibits significant variation with density. Furthermore, the optimal barrier height, determined from the most stable metastable structure and the lowest transition state structure, was found to be 5.06 eV, which is in excellent agreement with the experimental value of 5.13 eV. A detailed analysis of the experimental results for the Si-related diffusion coefficients in Si oxide films suggests that the films can be classified into at least two distinct types. Based on this observation, we propose that Si oxide films should not be simply treated as a single amorphous phase; rather, they should be systematically classified based on their structural characteristics from the perspective of quality assessment.

Acknowledgements

A part of this study has been supported by KAKENHI (22K18294). A part of calculations of this study is performed in the Super-computer Center of ISSP, University of Tokyo. Atomic structures are depicted with using VESTA [36].

Note

This paper was presented at the 10th International Symposium on Surface Science, Kitakyushu International Conference Center, Fukuoka, Japan, 20–24 October, 2024.

References

[1] H. Firdaus, T. Watanabe, M. Hori, D. Moraru, Y. Takahashi, A. Fujiwara, and Y. Ono, Nat. Commun. **9**, 4813 (2018).
[2] R. M. Jock, N. T. Jacobson, M. Rudolph, D. R. Ward, M. S. Carroll, and D. R. Luhman, Nat. Commun. **13**, 641 (2022).
[3] N. Ikarashi, K. Watanabe, and Y. Miyamoto, Phys. Rev. B **62**, 15989 (2000).
[4] C. Kaneta, Jpn. J. Appl. Phys. **35**, 1540 (1996).
[5] M. Boero, A. Pasquarello, J. Sarnthein, and R. Car, Phys. Rev. Lett. **78**, 887 (1997).
[6] T. Tsuchiya and Y. Ono, Jpn. J. Appl. Phys. **54**, 04DC01 (2015).
[7] A. Oshiyama, Jpn. J. Appl. Phys. **37**, L232 (1998).
[8] I. Kitagawa, T. Maruizumi, J. Ushio, K. Kubota, and M. Miyao, Jpn. J. Appl. Phys. **39**, 2021 (2000).
[9] S. M. Hu, Appl. Phys. Lett. **27**, 165 (1975).
[10] T. Y. Tan and U. Gösele, Appl. Phys. Lett. **39**, 86 (1981).
[11] H. Kageshima and K. Shiraishi, Phys. Rev. Lett. **81**, 5936 (1998).
[12] H. Kageshima, K. Shiraishi, and M. Uematsu, Jpn. J. Appl. Phys. **38**, L971 (1999).
[13] H. Kageshima, T. Akiyama, and K. Shiraishi, Mater. Sci. Semicond. Process. **162**, 107527 (2023).
[14] H. Kageshima, T. Akiyama, and K. Shiraishi, Jpn. J. Appl. Phys. **63**, 04SP08 (2024).
[15] M. Uematsu, H. Kageshima, Y. Takahashi, S. Fukatsu, K. M. Itoh, K. Shiraishi, and U. Gösele, Appl. Phys. Lett. **84**, 876 (2004).
[16] https://azuma.nims.go.jp.
[17] T. Yamasaki, A. Kuroda, T. Kato, J. Nara, J. Koga, T. Uda, K. Minami, and T. Ohno, Comput. Phys. Commun. **244**, 264 (2019).
[18] D. Vanderbilt, Phys. Rev. B **41**, 7892(R) (1990).
[19] J. P. Perdew, K. Burke, and M. Ernzerhof, Phys. Rev. Lett. **77**, 3865 (1996).
[20] H. J. Monkhorst and J. D. Pack, Phys. Rev. B **13**, 5188 (1976).
[21] K. Tatsumura, T. Watanabe, D. Yamasaki, T. Shimura, M. Umeno, and I. Ohdomari, Phys. Rev. B **69**, 085212 (2004).
[22] J. F. Shackelford, J. Non-Cryst. Solids **253**, 231 (1999).
[23] G. Malavasi, M. C. Menziani, A. Pedone, and U. Segre, J. Non-Cryst. Solids **352**, 285 (2006).
[24] H. Kageshima, M. Uematsu, T. Akiyama, and T. Ito, Jpn. J. Appl. Phys. **45**, 7672 (2006).
[25] T. Akiyama, K. Kawamoto, H. Kageshima, M. Uematsu, K. Nakamura, and T. Ito, Thin Solid Films **508**, 311 (2006).
[26] T. Akiyama, T. Ito, H. Kageshima, and M. Uematsu, Phys. Rev. B **77**, 115356 (2008).
[27] H. Ohta, T. Watanabe, and I. Ohdomari, Phys. Rev. B **78**, 155326 (2008).
[28] T. Akiyama, H. Kageshima, M. Uematsu, and T. Ito, Jpn. J. Appl. Phys. **47**, 7089 (2008).
[29] E. Kamiyama and K. Sueoka, J. Appl. Phys. **134**, 115301 (2023).
[30] S. Tsuneyuki and Y. Matsui, Phys. Rev. Lett. **74**, 3197 (1995).
[31] H. Kageshima, Y. Yajima, K. Shiraishi, and T. Endoh, Jpn. J. Appl. Phys. **58**, 111004 (2019).
[32] M. Uematsu, H. Kageshima, K. Shiraishi, M. Nagase, S. Horiguchi, and Y. Takahashi, Solid-State Electron. **48**, 1073 (2004).
[33] K. Yata and H. Kageshima, Jpn. J. Appl. Phys. **60**, 035504 (2021).
[34] F. J. Grunthaner and J. Maserjian, IEEE Trans. Nucl. Sci. **24**, 2108 (1977).
[35] E. Kobeda and E. A. Irene, J. Vac. Sci. Technol. B **5**, 15 (1987).
[36] K. Momma and F. Izumi, J. Appl. Cryst. **44**, 1272 (2011).